Electronic Supplementary Material (ESI) for Journal of Materials Chemistry A.

Supplementary information

Multipass inkjet printed planar methylammonium lead iodide perovskite solar cells

Florian Mathies,[a,b] Tobias Abzieher,[b] Adam Hochstuhl,[b] Konstantin Glaser,[b] Alexander Colsmann,[b] Ulrich W. Paetzold[c], Gerardo Hernandez-Sosa,[a,b] Uli Lemmer[b,c] and Aina Quintilla[d]

[a.] *InnovationLab GmbH, Speyererstr. 4, 69115 Heidelberg, Germany. E-mail: florian.mathies@kit.ede*
[b.] *Karlsruhe Institute of Technology, Light Technology Institute, Engesserstr. 13, 76131 Karlsruhe, Germany*
[c.] *Karlsruhe Institute of Technology, Institute of Microstructure Technology, Hermann-von-Helmholtz-Platz 1, 76344 Eggenstein-Leopoldshafen, Germany*
[d.] *Karlsruhe Institute of Technology, DFG-Center for Functional Nanostructures, Wolfgang-Gaede-Str. 1a, 76131 Karlsruhe, Germany*

I. Crystalization and drying of the printed perovskite layer

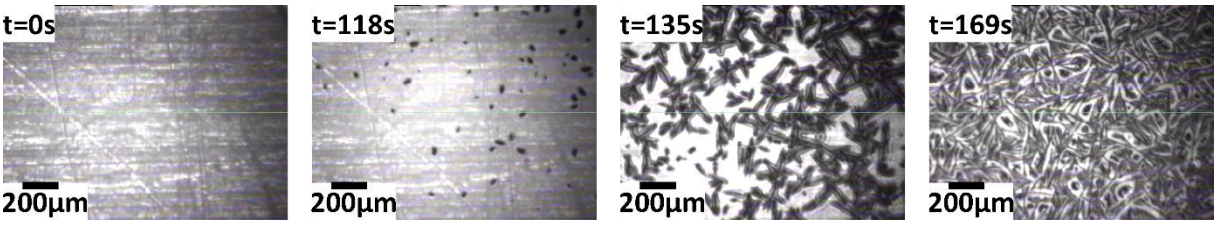

Figure S1: Microscope images at different points in time of the drying and crystallazation process omitting vacuum annealing. The images are taken from the Video S1.

Video S1: Additional video link of an inkjet printed perovskite layer onto TiO_2 omitting vacuum annealing. The time lapse video was recorded with the camera system of the used Dimatix DMP 2800 inkjet printer. The time lapse movie shows the crystallization process of a single layer of inkjet printed perovskite in 20x speed. In the beginning, you can see the slow evaporation of the high boiling point solvent (GBL). After approximately 2 min the first perovskite crystals are visible. The crystals grow very fast and after nearly 3 min the no further crystal growth is observable. The perovskite layer shows large crystal needles and a rough surface. Time lapse video: *Supplementary_TimelapseMovie_PerovskiteCrystallization.avi*

II. Surface topography of printed perovskite layers

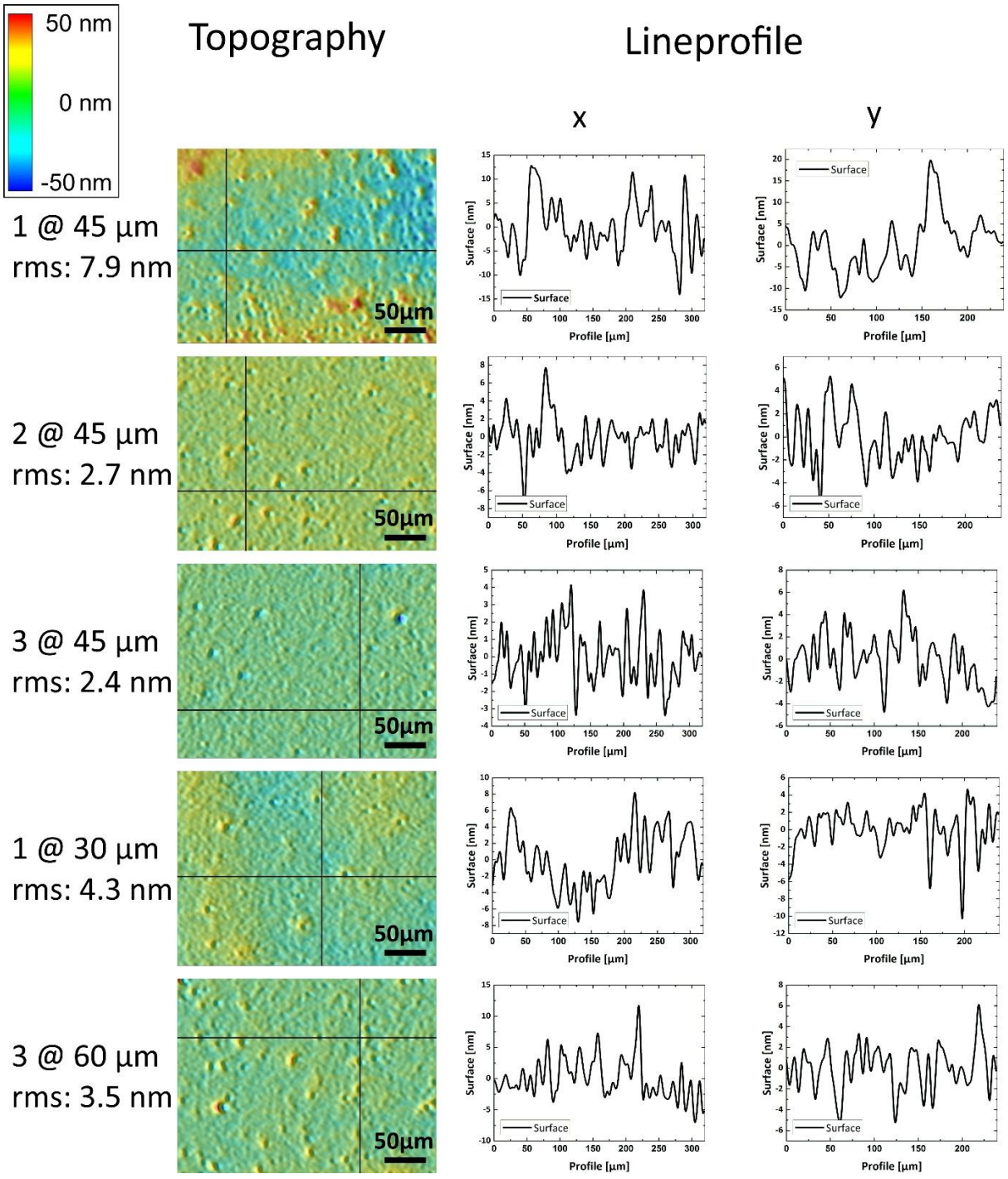

Figure S2: Surface Topography and its corresponding profiles of printed perovskite layers. The black lines in the white light interferometer images indicating where the profiles are taken. The x direction corresponds to the x axis of the predominant printing direction. The y direction corresponds to the y axis of the print direction, so perpendicular to the printed lines. From the images these line-by-line printing is not visible, which can be attributed to the usage of the high boiling point solvents, which lead to the formation of homogeneous wetfilms from wich the perovskite can crystallize.

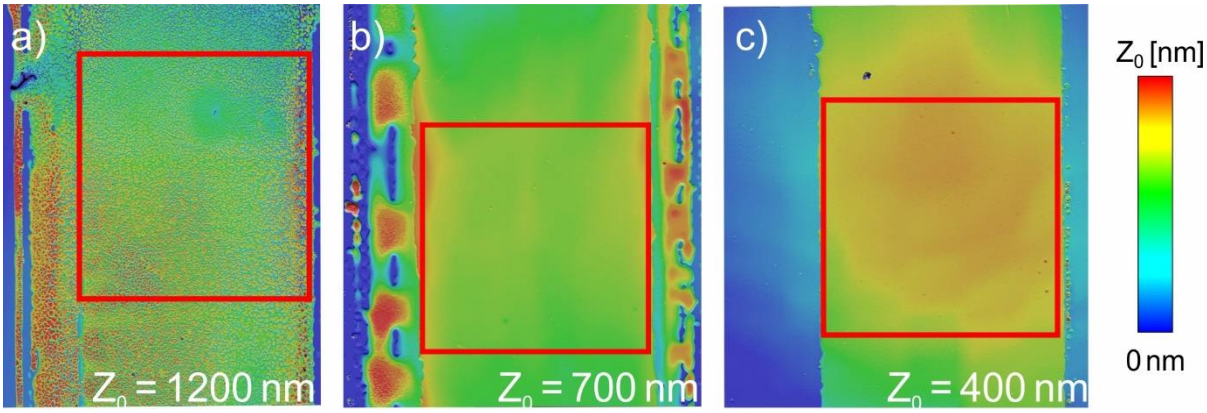

Figure S3: Comparison of white light interferometer images of the inkjet printed and spin cast devices. a) shows a typical inkjet printed device omitting vacuum annealing. b) depicts an inkjet printed device after 2 min vacuum annealing. c) shows a spin cast reference device. We observed no clear dependence of the LBIC mapping (Fig. 3c)) to the film thickness or layer roughness, shown in the sensofar images. Red rectangles are showing the later device area (3 mm x 3 mm).

Figure S3 depicts white light interferometer images of the inkjet printed perovskite layers which are analyzed in detail in Figure 4. To understand the fluctuations of the LBIC signal, the standard deviation about the mean value of the LBIC signal to the one from the topography values are compared. The results are shown in Table S1:

Table S1: Comparison of thickness variations, calculated from images in Figure S3, and LBIC signal fluctuations from Figure 4c).

Device	Vacuum annealing	Film thickness (nm)	Std. deviation (nm)	Std. deviation (%)	LBIC Std. deviation (%)
SC	-	460	4	0.9	6.5
3 @ 45 µm	w/	480	8	1.7	16.0
3 @ 45 µm	w/o	600[1]	260	43.3	27.6

Both, the spin cast and the vacuum annealed device show a very low thickness deviation of 0.9% and 1.7% respectively. The printed device omitting vacuum annealing shows a high fluctuation (43.3%) in film thickness with crystals of more than 1 µm height. The corresponding calculated LBIC signal deviations are 6.5, 16.0 and 27.6%. With this set of data, we were not able to attribute the LBIC fluctuations to the thickness fluctuations of the white light interferometer images.

[1] The printed layer omitting vacuum annealing shows no closed layer, so the film thickness is the mean value, calculated from the Figure S3a).

III. Crystal structure of printed perovskite layers

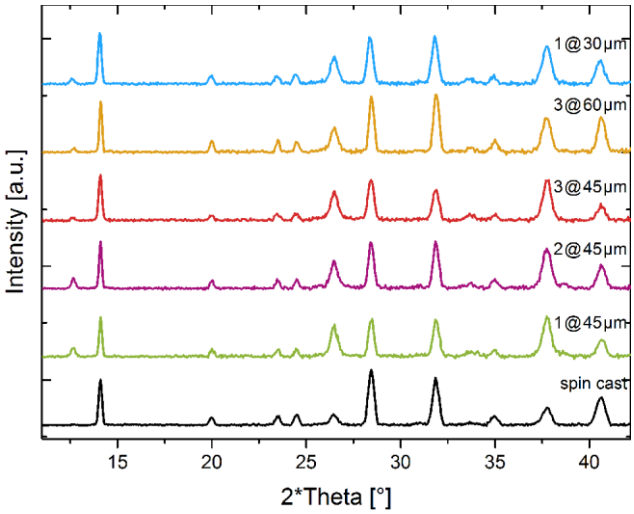

Figure S4: XRD patters of representative printed samples for different printing parameters. The PbI_2-peak at 14° becomes stronger for thinner printed layer thicknesses.

IV. Device Characteristics of printed perovskite layers

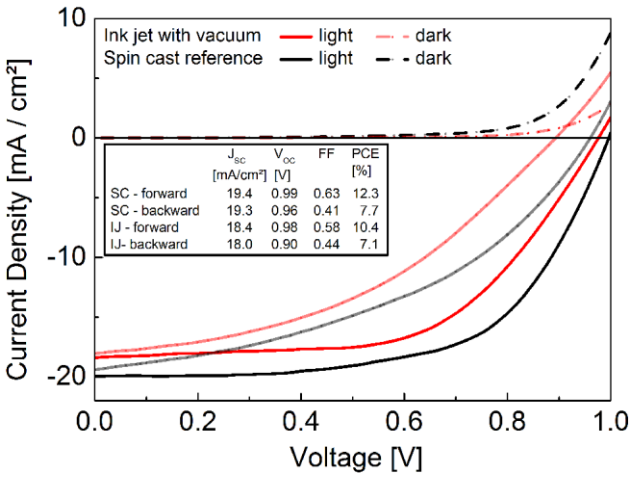

Figure S5: Observable hysteresis in J-V characteristics of inkjet printed (3 @ 45 µm) and spin cast reference device. The observed hysteresis can be attributed to the used perovskite precursor material and the HTL made of spiro-MeOTAD.

Table S2: Characteristic performance values of printed and spin cast devices for two batches.

Device	J_{SC} (mA / cm²)	V_{OC} (V)	FF	PCE (%)	# Devices
1 @ 45 µm	9.8 ± 1.1	0.86 ± 0.03	0.45 ± 0.05	3.8 ± 0.7	7
2 @ 45 µm	12.8 ± 1.3	0.89 ± 0.03	0.47 ± 0.04	5.3 ± 0.5	8
3 @ 45 µm	17.5 ± 0.9	0.99 ± 0.02	0.62 ± 0.04	10.7 ± 0.7	13
1 @ 30 µm	11.9 ± 1.3	0.89 ± 0.03	0.46 ± 0.04	4.8 ± 0.4	6
3 @ 60 µm	12.1 ± 0.8	0.86 ± 0.04	0.47 ± 0.04	4.9 ± 0.4	5
Spin cast	19.1 ± 0.8	1.00 ± 0.03	0.63 ± 0.02	12.2 ± 0.5	8